Topological Data Analysis and Use of Mapper for Cerebral Aneurysm Rupture Status Discrimination Based on 3-Dimensional Shape Analysis

Alexandra Lauric, PhD, Calvin G. Ludwig, MD, Adel M. Malek, MD, PhD

Cerebrovascular Hemodynamics Laboratory, Department of Neurosurgery, Tufts Medical Center and Tufts University School of Medicine, Boston, Massachusetts, USA

Correspondence: Adel M. Malek, MD, PhD, Department of Neurosurgery, Tufts Medical Center, 800 Washington St, Boston, MA 02111, USA. Email: amalek@tuftsmedicalcenter.org

Received, January 18, 2023; **Accepted,** April 26, 2023; **Published Online,** June 30, 2023.

© Congress of Neurological Surgeons 2023. All rights reserved.

BACKGROUND AND OBJECTIVES: Topological data analysis (TDA), which identifies patterns in data through simplified topological signatures, has yet to be applied to aneurysm research. We investigate TDA Mapper graphs (Mapper) for aneurysm rupture discrimination.

METHODS: Two hundred sixteen bifurcation aneurysms (90 ruptured) from 3-dimensional rotational angiography were segmented from vasculature and evaluated for 12 size/shape and 18 enhanced radiomics features. Using Mapper, uniformly dense aneurysm models were represented as graph structures and described by graph shape metrics. Mapper dissimilarity scores (MDS) were computed between pairs of aneurysms based on shape metrics. Lower MDS described similar shapes, whereas high MDS represented shapes that do not share common characteristics. Ruptured/unruptured average MDS scores (how "far" an aneurysm is shape-wise to ruptured/unruptured data sets, respectively) were evaluated for each aneurysm. Rupture status discrimination univariate and multivariate statistics were reported for all features.

RESULTS: The average MDS for pairs of ruptured aneurysms were significantly larger compared with unruptured pairs (0.055 ± 0.027 vs 0.039 ± 0.015, $P < .0001$). Low MDS suggest that, in contrast to ruptured aneurysms, unruptured aneurysms have similar shape characteristics. An MDS threshold value of 0.0417 (area under the curve [AUC] = 0.73, 80% specificity, 60% sensitivity) was identified for rupture status classification. Under this predictive model, MDS scores <0.0417 would identify unruptured status. MDS statistical performance in discriminating rupture status was similar to that of nonsphericity and radiomics Flatness (AUC = 0.73), outperforming other features. Ruptured aneurysms were more elongated ($P < .0001$), flatter ($P < .0001$), and showed higher nonsphericity ($P < .0001$) compared with unruptured. Including MDS in multivariate analysis resulted in AUC = 0.82, outperforming multivariate analysis on size/shape (AUC = 0.76) and enhanced radiomics (AUC = 0.78) alone.

CONCLUSION: A novel application of Mapper TDA was proposed for aneurysm evaluation, with promising results for rupture status classification. Multivariate analysis incorporating Mapper resulted in high accuracy, which is particularly important given that bifurcation aneurysms are challenging to classify morphologically. This proof-of-concept study warrants future investigation into optimizing Mapper functionality for aneurysm research.

KEY WORDS: 3D shape analysis, Intracranial aneurysms, Mapper, Topological data analysis, Rupture status

Neurosurgery 93:1285–1295, 2023 https://doi.org/10.1227/neu.0000000000002570

Topological data analysis (TDA) is a set of powerful tools for exploring complex data by investigating its intrinsic shape and identifying its structure patterns.[1] This quantification of data shape results in topological signatures that are visual representations highlighting some aspects of the data, presented in a simplified, easier to study format, most often as graph structures.

ABBREVIATIONS: EI, Ellipticity Index; **MDS,** Mapper dissimilarity score; **MRD,** Mapper ruptured dissimilarity; **MUD,** Mapper unruptured dissimilarity; **NSI,** nonsphericity; **TDA,** topological data analysis; **UI,** Undulation Index.

Supplemental digital content is available for this article at neurosurgery-online.com.

TDA have been increasingly used in medical research in recent years[2] in fields such as oncology,[3] pulmonary disease,[4] spinal cord and brain injury,[5] and cardiovascular medicine.[6] However, TDA has yet to be applied to aneurysm research.

Aneurysm morphology, such as size, shape, and angular characteristics, is still intensely studied as potential predictors of rupture risk.[7-11] In addition, research is focused on identifying more sophisticated tools for cerebral aneurysm evaluations to provide insight into the mechanism of aneurysm origination and rupture, such as the use of computation fluid dynamics,[12-17] fluid mechanics,[18,19] machine learning methods,[20-23] deep learning,[24,25] and radiomics.[26-28] Despite constant progress in the clinical management of cerebral

© Congress of Neurological Surgeons 2023. Unauthorized reproduction of this article is prohibited.

aneurysms, and despite the relative low risk of rupture for unruptured asymptomatic aneurysms, in the eventuality of rupture, aneurysmal subarachnoid hemorrhage carries a morbidity of 30%–50% and a mortality rate of 10%–20%.[29] Accordingly, identifying markers for rupture risk remains a focus of research and has high clinical value.

Here, we investigate the use of TDA Mapper graphs for aneurysm rupture discrimination. Mapper descriptors were evaluated on bifurcation aneurysms. Bifurcation aneurysms account for more than half of all ruptured aneurysms, have been shown to have different morphological and hemodynamic characteristics,[30,31] and have shown to be more difficult to classify morphologically.[7,28] TDA features proposed here were compared against well-known shape and size descriptors previously established in the literature[7,32] and against more recently introduced radiomics features for aneurysm evaluation.[26-28]

METHODS

Patient Selection

Consecutive high-resolution 3-dimensional (3D) angiographic data of patients undergoing cerebral angiography between 2001 and 2010 were reviewed for this study. All angiographic studies of patients with bifurcation aneurysms were included. Patient information, including rupture status, was retrieved from a prospectively maintained database. Consequently, volumetric data from 216 aneurysms were available for analysis. All imaging of the ruptured subset was obtained within 48 hours from rupture to avoid vasospasm onset.

This research was approved by the Institutional Review Board Ethics Committee. Patient consent was waived because of the retrospective nature of the study not affecting patient clinical care.

Cerebral Angiography and Data Processing

Three-dimensional catheter-based cerebral angiograms were obtained using either Philips Integris or Siemens Artis calibrated biplane systems, with secondary volume reconstruction over a predefined small region of interest window (resolution 0.14 mm), using the available clinical software package, to yield a three-dimensional volumetric data set.

Volumes were processed and analyzed using Amira visualization software platform version 5.3.3 (FEI) for segmentation of aneurysm and surrounding vasculature (Figure 1). The aneurysm dome was isolated and represented as a 3D triangular mesh model (Figure 1A). The aneurysm neck was identified for each aneurysm at the location where the aneurysm dome protrudes outward from the vessel, as described in the literature.[8,32,33] The inflow parent vessel was evaluated at 1 diameter proximal from the neck of the aneurysms, by placement of a cross-sectional plane. Both the neck plane and the parent vessel plane were represented as 3D triangular mesh models used to evaluate the neck and parent vessel size, respectively.

Angiographic volumes have arbitrary placement in the XYZ space because they are defined in the anatomic coordinate system (axial, sagittal, and coronal). Before Mapper analysis, rigid transformations were applied to each aneurysm dome to align its neck, by convention, to the XY plane (Figure 1A). In addition, all aneurysm models were remeshed using uniform meshing with an edge size of 0.1 mm. This preprocessing process performed in MATLAB (Mathworks) is automated, reproducible, and suitable for batch processing and enables comparison across all aneurysms using a consistent orientation.[28]

Established Size and Shape Feature Extraction

Size and shape parameters were automatically extracted from segmented aneurysmal domes using a previously described and validated MATLAB script.[33] The features evaluated have been previously described[28] and used in the literature for rupture status classification.[28,33] In brief, these features are **SizeMaximum** (aneurysm size), **HeightMaximum** (the largest distance between the center of the neck and the aneurysm surface), **WidthMaximum** (the largest distance orthogonal to the maximal height), **NeckAverage** (size of the aneurysmal neck), **ParentVesselSize** (size of the inflow vessel), **Height/Width** (the ratio of HeightMaximum/WidthMaximum), **AspectRatio** (the ratio of HeightMaximum/NeckAverage), **BottleneckFactor** (the ratio of WidthMaximum/NeckAverage), and **SizeRatio** (the ratio of HeightMaximum/ParentVesselSize). Three complex shape parameters, **Undulation Index**, **Ellipticity Index**, and **Nonsphericity**, were evaluated using the formulas introduced by Raghavan et al.[32]

Enhanced Radiomics Morphological Feature Extraction

PyRadiomics package, implemented in Python, was used.[34] Only shape parameters were considered because intensity-derived features are not relevant for 3DRA data used to generate the aneurysm volumetric representation.[26-28] The detailed information of radiomics features is available in the product documentation (http://www.radiomics.io/). The following enhanced radiomics descriptors have been evaluated, as previously described[28]: **Maximum3DDiameter** (aneurysm maximal size), the 3 axes of the enclosing ellipsoid (**MajorAxisLength, MinorAxisLength**, and **LeastAxisLength**), **Elongation** (the ratio of *MinorAxisLength/MajorAxisLength*), **Flatness** (the ratio of *LeastAxisLength/MajorAxisLength*), **SurfaceArea** (the total area of the shape), **MeshVolume** (the total volume of the shape), **SurfaceVolumeRatio** (surface to volume ratio), **Sphericity** (a measure of how close the shape resembles a sphere), **HeightOrthogonal** (the maximum between Maximum2DDiameterColumn and Maximum2DDiameterRow), **WidthOrthogonal** (the maximum dimension parallel to the neck as the Maximum2DDiameterSlice), orthogonal **Height/Width Orthogonal** (HeightOrthogonal/WidthOrthogonal), **SizeRatioHeightOrthogonal** (ratio between HeighOrthogonal and inflow size), and **SizeRatioMaximumDiameter** (ratio between Maximum3DDiameter and inflow size).

Mapper on 3D Shapes

The Python Mapper[35,36] application was run for each aneurysm. Mapper input was the 3D point cloud representing the mesh points on the surface of the aneurysm. The application was run with default settings[1]: Euclidean distance metric, eccentricity filter, uniform 1-d cover, 15 intervals, and 50% overlap. A detailed explanation of these metrics and additional technical details are available as supplementary material (**Supplemental Method**, http://links.lww.com/NEU/D878). Mapper output was a simplified shape representation as a graph. Figures 1B and 2A and 2B show examples of Mapper graphs corresponding to patient-derived and parametric shapes, respectively. In effect, an input shape is reduced to a graph representation, which allows for graph comparison analytics. Each graph is described by a shape metric, which details node cardinality, node weights, and distance between each pair of nodes in the graph (as a smooth approximation of the Hausdorff distance) (Figure 2C).

Graph comparison was evaluated from shape metrics. The comparison method between 2 shapes (pairs of aneurysms/corresponding graphs) takes the shape metric of the 2 graphs as input and computes an optimized version of the Gramov-Hausdorff distance as described by Memoli et al.[37] Consequently, pairs of aneurysms were analyzed, and a Mapper dissimilarity score was computed for all pairs of aneurysms based on

© Congress of Neurological Surgeons 2023. Unauthorized reproduction of this article is prohibited.

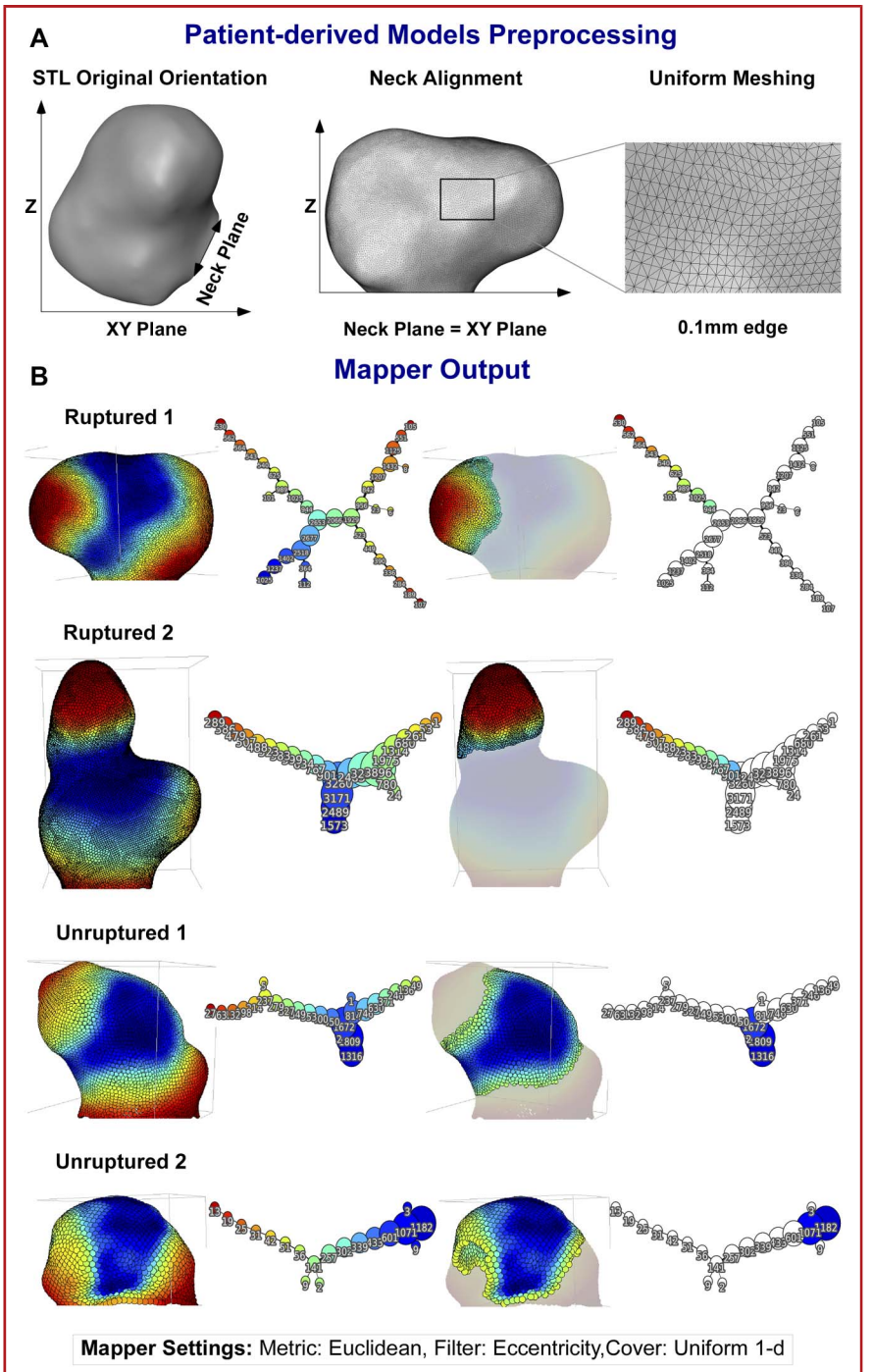


FIGURE 1. *3D models.* **A**, *Aneurysm dome was isolated from the segmented vasculature and represented as a 3D triangular mesh. Affine transformations were applied to all models such that, by convention, the aneurysm neck was aligned to the XY plane. Aneurysm models were remeshed using uniform meshing with an edge size of 0.1 mm.* **B**, *Mapper was applied to parametric and patient-derived models. Surface mesh points are clustered using the Euclidian metric and Eccentricity filter with 50% cluster overlap. Interactive software allows to isolate the points in each cluster for visualization and validation purposes. 3D, 3-dimensional.*

© Congress of Neurological Surgeons 2023. Unauthorized reproduction of this article is prohibited.

individual shape metrics, resulting in the data set dissimilarity matrix (Figure 2D). A low dissimilarity score describes a pair of aneurysms with similar shape characteristics. Pairs of identical shapes result in a dissimilarity score of 0 (Figure 2D).

From Mapper dissimilarity scores, 2 Mapper-derived features are evaluated for each aneurysm: **Mapper ruptured dissimilarity** (MRD) score and **Mapper unruptured dissimilarity** (MUD) score. The MRD of an aneurysm is computed as the average dissimilarity scores between this aneurysm and the entire subset of ruptured aneurysms. In effect, MRD describes how "far" an aneurysm is to the group of ruptured aneurysms, shape metric–wise. Similarly, the MUD of an aneurysm is computed as the average dissimilarity scores between this aneurysm and the entire subset of unruptured aneurysms. MUD describes how "far" an aneurysm is to the group of unruptured aneurysms shape metric–wise. Dissimilarly scores between an aneurysm and itself (which is 0, see Figure 2D) were not included when computing the average scores. Lower dissimilarity scores describe common shape characteristics, whereas high dissimilarity scores represent shapes that do not share common characteristics. Consequently, each aneurysm in the data set, regardless of its ruptured status, is described by 2 new shape features: MRD and MUD.

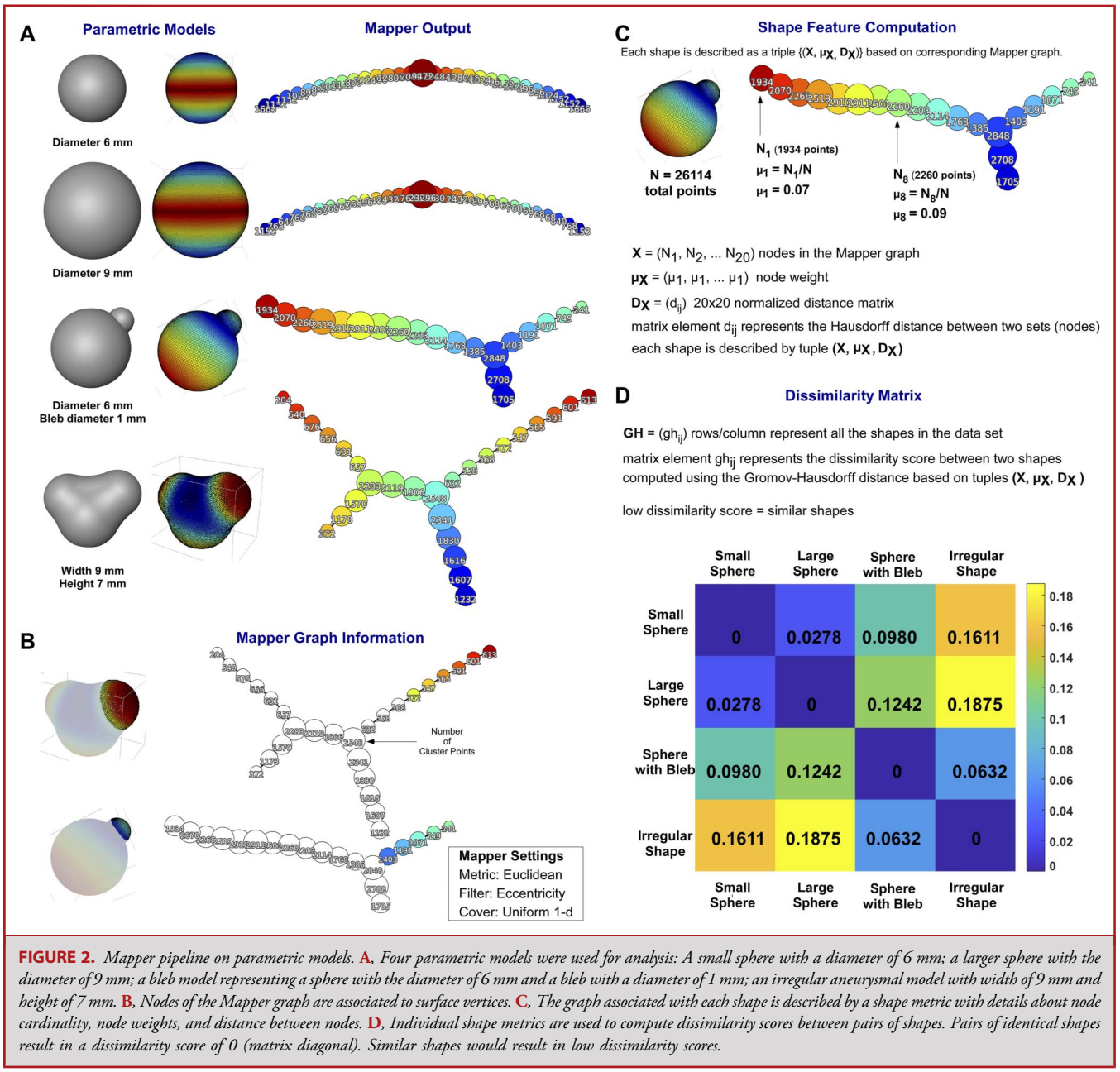


FIGURE 2. *Mapper pipeline on parametric models.* **A**, *Four parametric models were used for analysis: A small sphere with a diameter of 6 mm; a larger sphere with the diameter of 9 mm; a bleb model representing a sphere with the diameter of 6 mm and a bleb with a diameter of 1 mm; an irregular aneurysmal model with width of 9 mm and height of 7 mm.* **B**, *Nodes of the Mapper graph are associated to surface vertices.* **C**, *The graph associated with each shape is described by a shape metric with details about node cardinality, node weights, and distance between nodes.* **D**, *Individual shape metrics are used to compute dissimilarity scores between pairs of shapes. Pairs of identical shapes result in a dissimilarity score of 0 (matrix diagonal). Similar shapes would result in low dissimilarity scores.*

© Congress of Neurological Surgeons 2023. Unauthorized reproduction of this article is prohibited.

TABLE 1. Univariate Statistical Analysis for Mapper, Established, and Radiomics Parameters for Rupture Status Discrimination. Shown are Mean and SD

Parameters	Unruptured (N = 126)	Ruptured (N = 90)	*P* value	AUC
Age [y]	57.92 ± 12.61	54.77 ± 15.83	.10	0.56
Mapper descriptor				
MUD	0.039 ± 0.015	0.055 ± 0.027	<.0001[a]	0.73
MRD	0.053 ± 0.012	0.053 ± 0.015	.87	0.54
Established size and shape descriptors				
SizeMaximum [mm]	7.07 ± 2.88	7.93 ± 3.56	.05	0.56
Area [mm^2]	98.17 ± 84.65	115.31 ± 119.5	.21	0.52
Volume [mm^3]	111.32 ± 141.27	135.98 ± 216.64	.31	0.48
HeightMaximum [mm]	5.53 ± 2.53	6.5 ± 3.09	.01[a]	0.59
WidthMaximum [mm]	5.71 ± 2.37	5.67 ± 2.57	.90	0.52
Height/width	0.98 ± 0.24	1.17 ± 0.28	<.0001[a]	0.71
AspectRatio	1.39 ± 0.53	1.85 ± 0.66	<.0001[a]	0.72
BottleneckFactor	1.53 ± 0.41	1.83 ± 0.55	<.0001[a]	0.68
SizeRatio	2.24 ± 1.1	3.04 ± 1.53	<.0001[a]	0.67
NSI	0.18 ± 0.1	0.24 ± 0.07	<.0001[a]	0.73
EI	0.26 ± 0.02	0.27 ± 0.02	<.0001[a]	0.67
UI	0.11 ± 0.1	0.14 ± 0.09	.02[a]	0.65
Enhanced radiomics descriptors				
Elongation	0.77 ± 0.13	0.66 ± 0.13	<.0001[a]	0.72
Flatness	0.65 ± 0.12	0.56 ± 0.11	<.0001[a]	0.73
LeastAxisLength [mm]	3.94 ± 1.58	3.86 ± 1.79	.72	0.53
MajorAxisLength [mm]	6.16 ± 2.65	7.1 ± 3.35	.02[a]	0.58
Maximum2DDiameterColumn [mm]	6.26 ± 2.56	6.89 ± 3.31	.08	0.54
Maximum2DDiameterRow [mm]	6.45 ± 2.64	7.06 ± 3.30	.30	0.51
Maximum2DDiameterSlice [mm]	6.21 ± 2.55	6.54 ± 3.09	.32	0.53
Maximum3DDiameter [mm]	7.13 ± 2.89	8.01 ± 3.58	.04[a]	0.56
MeshVolume [mm^3]	113.53 ± 142.49	136.15 ± 218.85	.35	0.50
MinorAxisLength [mm]	4.62 ± 1.8	4.56 ± 2.04	.83	0.53
Sphericity	0.8 ± 0.05	0.77 ± 0.06	<.0001[a]	0.67
SurfaceArea [mm^2]	124.05 ± 102.49	142.53 ± 147.15	.29	0.51
SurfaceVolumeRatio [1/mm]	1.69 ± 0.78	1.75 ± 0.73	.63	0.53
HeightOrthogonal	6.77 ± 2.73	7.46 ± 3.33	.09	0.56
WidthOrthogonal	6.21 ± 2.55	6.54 ± 3.09	.39	0.52
Height/width orthogonal	1.06 ± 0.17	1.18 ± 0.24	.01[a]	0.57

© Congress of Neurological Surgeons 2023. Unauthorized reproduction of this article is prohibited.

TABLE 1. Continued.

Parameters	Unruptured (N = 126)	Ruptured (N = 90)	*P* value	AUC
SizeRatioHeightOrthogonal	2.72 ± 1.44	3.28 ± 1.49	.002[a]	0.62
SizeRatioMaximumDiameter	2.87 ± 1.19	3.52 ± 1.54	.0001[a]	0.63

AUC, area under the curve; EI, Elipticity Index; MRD, Mapper ruptured dissimilarity; MUD, Mapper unruptured dissimilarity; NSI, Nonsphericity; UI, Undulation Index.
[a]Indicates statistical significance (assumed for $P < .05$). AUC, area under the ROC curve.
Reprinted from Lauric et al,[28] Copyright 2021, with permission from Elsevier.

Parametric Models

To provide an intuitive understanding of Mapper-derived parameters, 4 parametric representations of simple aneurysm-like shapes were created: (1) small sphere with a diameter of 6 mm, (2) larger sphere with a diameter of 9 mm, (3) small sphere with a diameter of 6 mm and a 1-mm lateral bleb, and (4) irregular-shaped aneurysm with a **SizeMaximum** of 9 mm and a **HeightMaximum** of 7 mm (Figure 2A). These parametric shapes were processed in a similar fashion to the patient-derived aneurysms.

Statistical Analysis

Statistical analysis was performed using JMP statistical software (version Pro 16.2, SAS Institute). Each variable was tested independently using the Student *t*-test analysis to determine performance in discriminating ruptured status. Statistical significance was assumed to be $P < .05$. Receiver operating characteristics curve was evaluated, and discrimination accuracy was determined using the area under the curve (AUC) index. Multivariate statistical analysis was evaluated using stepwise forward feature selection, including only those parameters that were statistically significant in univariate analysis ($P < .05$).

RESULTS

Patient Demographics

A total of 216 bifurcation aneurysms (90 ruptured, 151 female patients) were analyzed. The distribution of aneurysms by location is as follows: 94 anterior communicating arteries, 61 middle cerebral arteries, 24 basilar arteries, 17 internal carotid artery bifurcations, 12 posterior communicating arteries, 6 superior cerebellar arteries, and 2 posterior inferior cerebellar arteries. There was no statistically significant difference in age between the ruptured and unruptured subgroups (Table 1).

Established Parameters

As presented in Table 1, most established size and shape parameters were statistically significant in predicting rupture status, except for SizeMaximum, Area, Volume, and WidthMaximum. Nonsphericity ($P < .0001$, AUC = 0.73), AspectRatio ($P < .0001$, AUC = 0.72), and Height/Width ($P < .0001$, AUC = 0.71) were identified as the best among established parameters for rupture status discrimination in univariate analysis. Ruptured aneurysms had significantly higher nonsphericity (0.24 ± 0.07 vs 0.19 ± 0.1), larger aspect ratio (1.85 ± 0.66 vs 1.39 ± 0.53), and greater height/width (1.17 ± 0.28 vs 0.98 ± 0.24) compared with unruptured aneurysms.

Enhanced Radiomics

Elongation ($P < .0001$, AUC = 0.72) and Flatness ($P < .0001$, AUC = 0.73) were the best performers among radiomics features (Table 2). Ruptured aneurysms had significantly lower Elongation (0.66 ± 0.13 vs 0.77 ± 0.13) and Flatness (0.56 ± 0.11 vs 0.65 ± 0.12) compared with unruptured aneurysms. In addition, enhanced radiomics HeightWidth (1.18 ± 0.24 vs 1.06 ± 0.17), SizeRatioHeightOrthogonal (3.28 ± 1.49 vs 2.72 ± 1.44), and SizeRatioMaximumDiameter (3.52 ± 1.54 vs 2.87 ± 1.19) were significantly higher in ruptured bifurcation aneurysms.

Mapper on Parametric Models

As shown in Figure 2D, dissimilarity scores between identical pairs of shapes are 0 (the dissimilarity matrix diagonal). Pairs of small/large spheres have nonzero low dissimilarity scores. Although both are spheres, differences in size are reflected in different node weights, which contribute to the computation of the shape metric. The highest dissimilarity scores are between the perfect spheres and the irregular shapes. Interestingly, based on dissimilarity scores, the sphere with a bleb has shape characteristics that are closer to the irregular shape than the 2 perfect spheres.

Mapper on Patient-Derived Models

Figure 3 shows the dissimilarity matrix for the set of aneurysms (Figure 3A) and samples of the Mapper output for ruptured and unruptured aneurysms (Figure 3B). Pairs of ruptured aneurysms have statistically significantly higher dissimilarity scores compared with pairs of unruptured aneurysms. This shows that the group of unruptured aneurysms share common shape characteristics to a greater extent than the group of ruptured aneurysms. This is also reflected in MUD being statistically significant between ruptured and unruptured aneurysms (0.055 ± 0.027 vs 0.039 ± 0.015, $P < .0001$, AUC = 0.73), in contrast to MRD (0.053 ± 0.015 vs 0.053 ± 0.012, $P = .87$, AUC = 0.54) as shown in Figure 3C. Under this model, an unruptured aneurysm would have low MUD (similar in shape to other unruptured aneurysms) and high MRD (not similar to ruptured aneurysms). By contrast, a ruptured aneurysm will not only have high MUD (not similar to the group of unruptured aneurysms) but also high MRD (the group of ruptured aneurysms do not share similar shape characteristics).

MUD showed the same performance as Nonsphericity and Flatness (AUC = 0.73) in discriminating rupture status and

© Congress of Neurological Surgeons 2023. Unauthorized reproduction of this article is prohibited.

TABLE 2. Multivariate Analysis for All Groups of Features

Features	OR [95% CI]	*P* value	AUC
Established size/shape features			
BottleneckFactor	0.76, [0.22, 2.63]	.42	0.76
SizeRatio	1.26, [0.94, 1.69]	.13	
EllipticityIndex	52 913.92, [5.52, 5.06e+8]	.0005	
UndulationIndex	0.0005, [6.54e−7, 0.46]	.07	
Nonsphericity	1.02e+12, [2600.29, 3.98e+20]	.08	
Enhanced radiomics			
Elongation	0.05, [0.0005, 5.98]	.15	0.78
Flatness	0.007, [3.65e−5, 1.57]	.07	
MajorAxisLength	0.64, [0.50, 0.81]	.0006	
SizeRatioHeightOrthogonal	0.31, [0.05, 1.71]	.19	
SizeRatioMaximumDiameter	8.79, [1.53, 50.41]	.01	
Mapper and established features			
MUD	2.58e+10, [65.19, 1.02e+19]	.009	0.79
HeightMaximum	0.81, [0.66, 0.99]	.04	
AspectRatio	2.47, [1.14, 5.37]	.02	
SizeRatio	1.61, [1.03, 2.51]	.03	
ElipticityIndex	1 018 166, [0.03, 3.23e+13]	.12	
Mapper and enhanced radiomics			
MUD	5.58e+15, [2 151 975, 1.45e+25]	.0003	0.81
Flatness	0.007, [0.00026, 0.2173]	.003	
MajorAxisLength	0.57, [0.442278, 0.755352]	<.0001	
SizeRatioHeightOrthogonal	0.26, [0.045451, 1.568566]	.14	
SizeRatioMaximumDiameter	12.30, [1.972174, 76.7471]	.006	
All features			
MUD	8.58e+13, [26 083, 2.82e+23]	.002	0.82
AspectRatio	2.030154, [0.97, 4.24]	.05	
Flatness	0.017176, [0.0004, 0.59]	.02	
MajorAxisLength	0.581172, [0.44, 0.76]	<.0001	
SizeRatioMaximumDiameter	3.122439, [1.79, 5.44]	<.0001	

MUD, Mapper unruptured dissimilarity; OR, odds ratio.
Only those parameters that were statistically significant in univariate analysis were included in multivariate analysis. AUC, area under the ROC curve. Odds ratio (OR) and 95% CI are provided.

outperformed all other features (Table 1, Figure 4A). A threshold value of MUD = 0.0417 (AUC = 0.73, 80% specificity, 60% sensitivity) was identified for rupture status classification. Under this predictive model, MUD scores less than 0.0417 would identify aneurysms with an unruptured label, whereas MUD scores more than 0.0417 would identify aneurysms with a ruptured label.

© Congress of Neurological Surgeons 2023. Unauthorized reproduction of this article is prohibited.

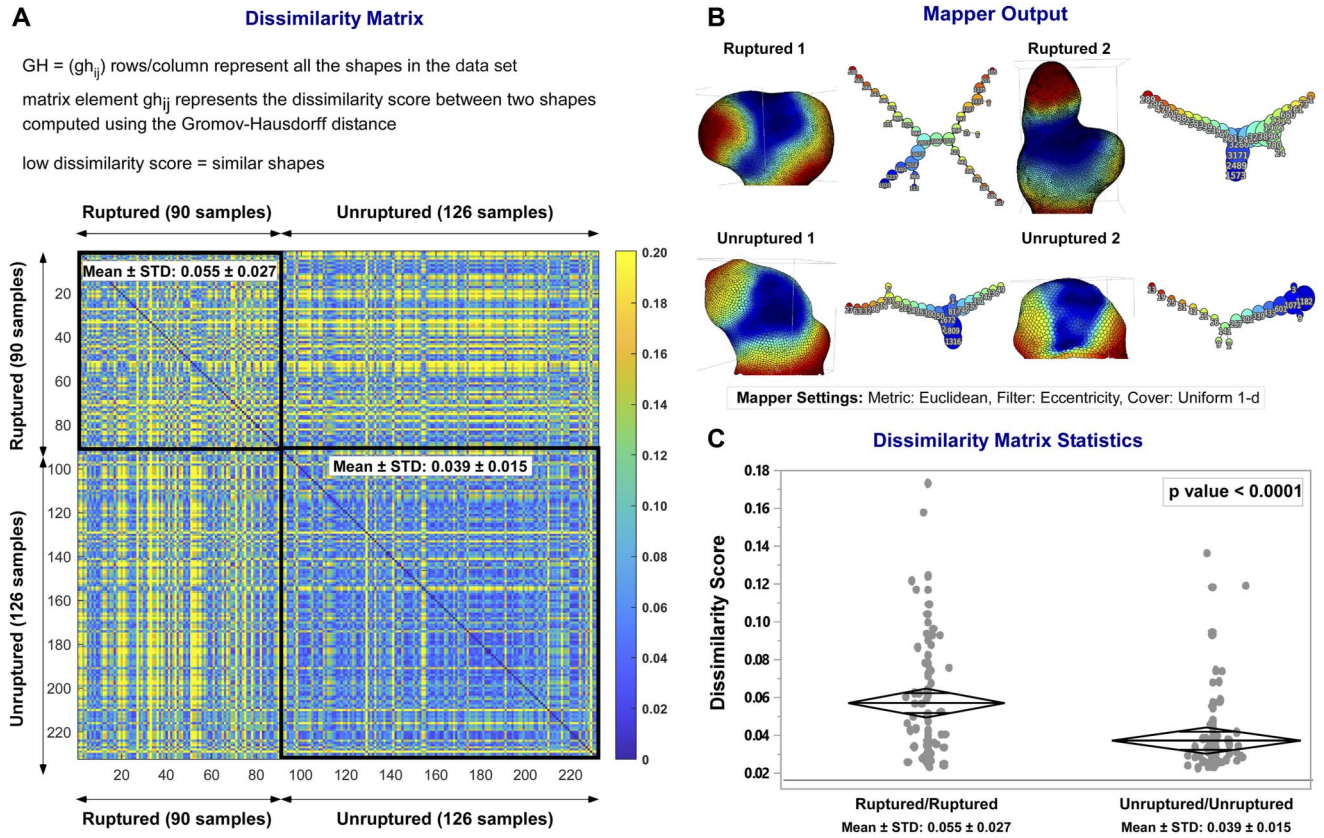


FIGURE 3. *Data set dissimilarity matrix.* **A**, *Pairs of aneurysms were analyzed, and a dissimilarity score was computed for all pairs of aneurysms based on individual shape metrics, resulting in the data set dissimilarity matrix.* **B**, *Mapper output on 2 ruptured and 2 unruptured aneurysmal shapes. Ruptured aneurysms result in more complex topological graphs, whereas unruptured aneurysms result in graphs with simple node connections. Our results show that the group of unruptured aneurysms has lower dissimilarity scores, describing common shape characteristics, whereas the group of ruptured aneurysm has higher dissimilarity scores, indicative of less shape homogeneity.* **C**, *Pairs of ruptured aneurysms have significantly higher dissimilarity scores compared with pairs of unruptured aneurysms.*

Additional analysis based on aneurysmal size stratification is provided as supplementary material (**Supplemental Table**, http://links.lww.com/NEU/D879). This evaluation on groups of small, medium, and large aneurysms showed that MUD has a good comparative performance independent of the aneurysmal size.

Multivariate Analysis

Multivariate statistical analysis was evaluated using stepwise forward feature selection for Mapper, established and enhanced radiomics features (Table 2). Only those parameters that were statistically significant in univariate analysis were included in multivariate analysis. Multivariate statistical analysis revealed that including MUD in the analysis (MUD, AspectRatio, Flatness, MajorAxisLength, and SizeRatioMaximumDiameter, AUC = 0.82) outperformed multivariate analysis using established descriptors (AUC = 0.76) or enhanced radiomics (AUC = 0.78) alone (Table 2, Figure 4B). For all sets of features, adding additional descriptors to the multivariate set did not result in improved statistical performance.

DISCUSSION

TDA methods are increasingly being proposed for investigation of complex medical data.[2-6] TDA works by representing data points (including 3D cloud points) as topological signatures, highlighting some aspect of the data, often finding structures in the data that might be overlooked by other methods. Although machine learning methods have been proposed for the evaluation and classification of cerebral aneurysms,[20-23] TDA has yet to be applied to this field.

Here, we proposed a novel use of TDA Mapper graphs for aneurysm rupture status discrimination. Mapper provides a one-dimensional representation of each aneurysm in graph format, allowing for graph operations (such as distance calculations and shape comparison). The method was applied to bifurcation aneurysms, previously shown to be more difficult to classify morphologically. Specifically, compared with sidewall aneurysms, many size and shape descriptors,[7] but also newly introduced radiomics features,[28] fail to discriminate with high accuracy between ruptured and unruptured aneurysms. Our results showed that Mapper-derived MUD

© Congress of Neurological Surgeons 2023. Unauthorized reproduction of this article is prohibited.

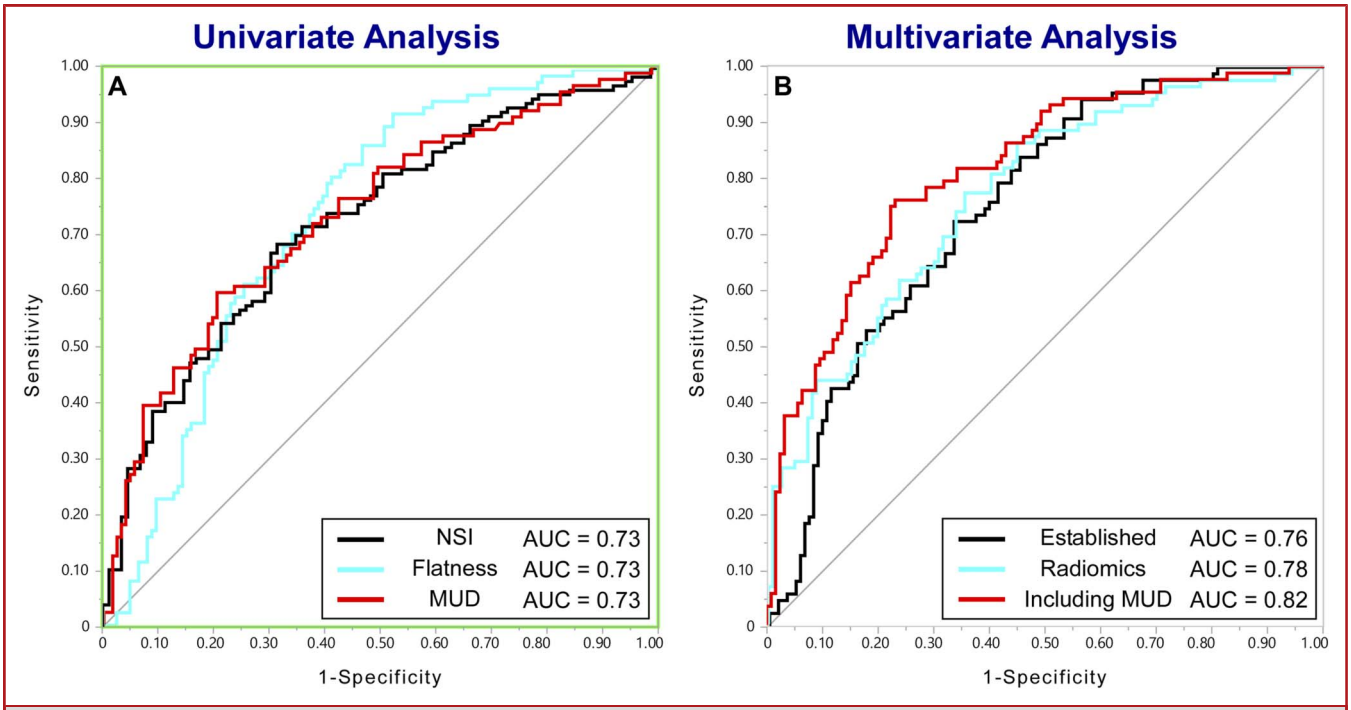


FIGURE 4. *Comparison of ROC curves.* **A**, *ROC curves corresponding to univariate analysis of best ruptured status discriminators Nonsphericity, Flatness, and MUD, respectively.* **B**, *ROC curves corresponding to multivariate analysis when considering established features, enhanced radiomics features, and all features including MUD, respectively. AUC indicates the area under the ROC curve. AUC, area under the curve; MUD, Mapper unruptured dissimilarity; NSI, Nonsphericity; ROC, receiver operating characteristics.*

(AUC = 0.73) performed as well as Nonsphericity and Flatness, which were the best rupture status discriminator from the groups of established and radiomics features, respectively. Incorporating MUD to multivariate analysis resulted in increased performance for rupture status discrimination (AUC = 0.82). To the best of our knowledge, this is the highest reported accuracy for rupture status discrimination on bifurcation aneurysms.

Mapper-derived parameters, MRD and MUD, describe how "far" (dissimilar) an aneurysm is to the groups of ruptured and unruptured aneurysms, respectively. The results suggest that the group of unruptured aneurysms have similar shape characteristics (low MUD), but ruptured aneurysms do not. That is, whereas unruptured aneurysms are a homogenous group shape-wise, ruptured aneurysms are not. Specifically, under this model, an unruptured aneurysm would have low MUD (similar in shape to other unruptured aneurysms) and high MRD (different from ruptured aneurysms). By contrast, a ruptured aneurysm will have high MUD and MRD (different from other aneurysms regardless of ruptured status). In effect, the method is answering the question "is this an unruptured aneurysm?" It describes ruptured aneurysms as not being unruptured. This important insight regarding the aneurysmal data set, that was highlighted by Mapper analysis, could explain why many size and shape aneurysmal feature fail to discriminate rupture status on bifurcation aneurysms and would inform future research and clinical studies evaluating aneurysm morphology.

In this proof-of-concept analysis, Mapper available software was run using default settings for metric, filter, cover, number of intervals, and percentage overlap. Even so, the results contribute to improved rupture status discrimination, which warrants future research into optimizing Mapper setting specific for aneurysm research.

Study Limitations

This study is retrospective in nature and used for classification of rupture status. As all retrospective studies, it does not predict aneurysmal rupture but identifies features that can discriminate between aneurysms with known ruptured or unruptured labels. Retrospective analysis relies on the hypothesis that aneurysm morphology does not change after rupture. Previous research suggests this is indeed the case,[38] consistent with intraoperative findings; however, conclusive data on this subject are still to be established. If aneurysmal morphology was to dramatically change after rupture, the current class of analysis might not be helpful. It should be noted that the association between aneurysm morphology and ruptured status suggests correlation, but not causation, a limitation shared with all similar research. Prospective studies, in which the evolution of unruptured aneurysms is followed over time, would be required to evaluate the clinical relevance of this proposed use of Mapper for morphological analysis.

© Congress of Neurological Surgeons 2023. Unauthorized reproduction of this article is prohibited.

These results were evaluated on bifurcation aneurysms only to avoid confounding factors, such as morphological differences between sidewall and bifurcation lesions.[30,31] It remains to be determined by future research whether these findings are true for all aneurysms.

It should be noted that because Mapper-derived features describe aneurysm morphology, in this study, we only compared their performance with other previously used morphological features. Additional analysis, which will include features such as computational fluid dynamics parameters and clinical history and examination data (such as arterial hypertension, smoking, alcohol consumption, and family history of aneurysmal subarachnoid hemorrhage), will be the focus of future investigation.

CONCLUSION

A novel application of Mapper topological analysis is proposed for aneurysm shape evaluation, with promising results for rupture status classification. Dissimilarity scores are defined to describe how different aneurysm shape characteristics are. Pairs of unruptured aneurysms had significantly smaller dissimilarity scores compared with those between pairs of ruptured aneurysms. Low dissimilarity scores suggest unruptured, but not ruptured, aneurysms have similar shape characteristics. Univariate analysis based on MUD scores had same performance as Nonsphericity and Flatness (AUC = 0.73) in discriminating rupture status and outperformed all other evaluated features. A threshold value of 0.0417 dissimilarity score (AUC = 0.73, 80% specificity, 60% sensitivity) was identified for rupture status classification. Multivariate analysis incorporating Mapper resulted in high accuracy (AUC = 0.82), particularly important given that bifurcations aneurysms are challenging to classify morphologically. To the best of our knowledge, this is the best reported accuracy for bifurcation aneurysms. This proof-of-concept study using Euclidean eccentricity warrants future investigation into additional Mapper metrics and filter functions for aneurysm research.

Funding

This study did not receive any funding or financial support.

Disclosures

The authors have no personal, financial, or institutional interest in any of the drugs, materials, or devices described in this article.

REFERENCES

1. Munch E. A user's guide to topological data analysis. *J Learn Anal*. 2017;4(2):47-61.
2. Joshi M, Joshi D. A survey of topological data analysis methods for big data in healthcare intelligence. *Int J Appl Eng Res*. 2019;14(2):584-588.
3. Bukkuri A, Andor N, Darcy IK. Applications of topological data analysis in oncology. Review. *Front Artif Intell*. 2021;4(38):659037.
4. Belchi F, Pirashvili M, Conway J, Bennett M, Djukanovic R, Brodzki J. Lung topology characteristics in patients with chronic obstructive pulmonary disease. *Sci Rep*. 2018;8(1):5341.
5. Nielson JL, Paquette J, Liu AW, et al. Topological data analysis for discovery in preclinical spinal cord injury and traumatic brain injury. *Nat Commun*. 2015;6(1):8581.
6. Tokodi M, Shrestha S, Bianco C, et al. Interpatient similarities in cardiac function. *JACC Cardiovasc Imaging*. 2020;13(5):1119-1132.
7. Baharoglu MI, Lauric A, Gao B-L, Malek AM. Identification of a dichotomy in morphological predictors of rupture status between sidewall- and bifurcation-type intracranial aneurysms. *J Neurosurg*. 2012;116(4):871-881.
8. Xiang J, Natarajan SK, Tremmel M, et al. Hemodynamic-morphologic discriminants for intracranial aneurysm rupture. *Stroke*. 2011;42(1):144-152.
9. Rajabzadeh-Oghaz H, Varble N, Shallwani H, et al. Computer-assisted three-dimensional morphology evaluation of intracranial aneurysms. *World Neurosurg*. 2018;119:e541-e550.
10. Piccinelli M, Steinman DA, Hoi Y, Tong F, Veneziani A, Antiga L. Automatic neck plane detection and 3D geometric characterization of aneurysmal sacs. *Ann Biomed Eng*. 2012;40(10):2188-2211.
11. Dhar S, Tremmel M, Mocco J, et al. Morphology parameters for intracranial aneurysm rupture risk assessment. *Neurosurgery*. 2008;63(2):185.
12. Lauric A, Hippelheuser JE, Malek AM. Induction of aneurysmogenic high positive wall shear stress gradient by wide angle at cerebral bifurcations, independent of flow rate. *J Neurosurg*. 2019;131(2):442-452.
13. Zhou G, Zhu Y, Yin Y, Su M, Li M. Association of wall shear stress with intracranial aneurysm rupture: systematic review and meta-analysis. *Sci Rep*. 2017;7(1):5331.
14. Suzuki T, Stapleton CJ, Koch MJ, et al. Decreased wall shear stress at high-pressure areas predicts the rupture point in ruptured intracranial aneurysms. *J Neurosurg*. 2019;132(4):1116-1122.
15. Xiang J, Antiga L, Varble N, et al. AView: an image-based clinical computational tool for intracranial aneurysm flow visualization and clinical management. *Ann Biomed Eng*. 2016;44(4):1085-1096.
16. Xiang J, Yu J, Choi H, et al. Rupture Resemblance Score (RRS): toward risk stratification of unruptured intracranial aneurysms using hemodynamic–morphological discriminants. *J Neurointerv Surg*. 2015;7(7):490-495.
17. Rajabzadeh-Oghaz H, Waqas M, Veeturi SS, et al. A data-driven model to identify high-risk aneurysms and guide management decisions: the Rupture Resemblance Score. *J Neurosurg*. 2020;135(1):9-16.
18. Torii R, Oshima M, Kobayashi T, Takagi K, Tezduyar TE. Fluid–structure interaction modeling of blood flow and cerebral aneurysm: significance of artery and aneurysm shapes. *Comput Methods Appl Mech Eng*. 2009;198(45):3613-3621.
19. Cebral JR, Vazquez M, Sforza DM, et al. Analysis of hemodynamics and wall mechanics at sites of cerebral aneurysm rupture. *J Neurointerv Surg*. 2015;7(7):530-536.
20. Amigo N, Valencia A, Wu W, Patnaik S, Finol E. Cerebral aneurysm rupture status classification using statistical and machine learning methods. *Proc Inst Mech Eng H*. 2021;235(6):655-662.
21. Heo J, Park SJ, Kang S-H, Oh CW, Bang JS, Kim T. Prediction of intracranial aneurysm risk using machine learning. *Sci Rep*. 2020;10(1):6921.
22. Shi Z, Chen GZ, Mao L, et al. Machine learning-based prediction of small intracranial aneurysm rupture status using CTA-derived hemodynamics: a multicenter study. *Am J Neuroradiol*. 2021;42(4):648-654.
23. Tanioka S, Ishida F, Yamamoto A, et al. Machine learning classification of cerebral aneurysm rupture status with morphologic variables and hemodynamic parameters. *Radiol Artif Intell*. 2020;2(1):e190077.
24. Li G, Song X, Wang H, et al. Prediction of cerebral aneurysm hemodynamics with porous-medium models of flow-diverting stents via deep learning. Original research. *Front Physiol*. 2021;12:733444.
25. Yang H, Cho K-C, Kim J-J, Kim JH, Kim YB, Oh JH. Rupture risk prediction of cerebral aneurysms using a novel convolutional neural network-based deep learning model. *J Neurointerv Surg*. 2022;15(2):200-204.
26. Liu Q, Jiang P, Jiang Y, et al. Prediction of aneurysm stability using a machine learning model based on pyradiomics-derived morphological features. *Stroke*. 2019;50(9):2314-2321.
27. Ludwig CG, Lauric A, Malek JA, Mulligan R, Malek AM. Performance of Radiomics derived morphological features for prediction of aneurysm rupture status. *J Neurointerv Surg*. 2020;13(8):755-761.
28. Lauric A, Ludwig CG, Malek AM. Enhanced Radiomics for prediction of rupture status in cerebral aneurysms. *World Neurosurg*. 2022;159:e8-e22.
29. van Gijn J, Kerr RS, Rinkel GJE. Subarachnoid haemorrhage. *Lancet*. 2007;369(9558):306-318.

© Congress of Neurological Surgeons 2023. Unauthorized reproduction of this article is prohibited.

30. Valen-Sendstad K, Mardal K-A, Steinman DA. High-resolution CFD detects high-frequency velocity fluctuations in bifurcation, but not sidewall, aneurysms. *J Biomech*. 2013;46(2):402-407.
31. Qiu T, Xing H. Morphological distinguish of rupture status between sidewall and bifurcation cerebral aneurysms. *Int J Morphol*. 2014;3(32):9.
32. Raghavan ML, Ma B, Harbaugh RE. Quantified aneurysm shape and rupture risk. *J Neurosurg*. 2005;102(2):355-362.
33. Lauric A, Baharoglu MI, Malek AM. Ruptured status discrimination performance of aspect ratio, height/width, and bottleneck factor is highly dependent on aneurysm sizing methodology. *Neurosurgery*. 2012;71(1):38-46.
34. van Griethuysen JJM, Fedorov A, Parmar C, et al. Computational radiomics system to decode the radiographic phenotype. *Cancer Res*. 2017;77(21):e104-e107.
35. Müllner D, Babu A. *Python Mapper: An Open-Source Toolchain for Data Exploration, Analysis and Visualization*. 2013. Accessed June 2, 2021. http://danifoldnet/mapper.
36. Singh G, Mémoli F, Carlsson GE. Topological methods for the analysis of high dimensional data sets and 3D object recognition. *PBG@Eurographics*. 2007;2:91-100.
37. Memoli F. On the use of Gromov-Hausdorff distances for shape comparison. *Presented at: Eurographics Symposium on Point-Based Graphics*; 2007.
38. Asari S, Ohmoto T. Natural history and risk factors of unruptured cerebral aneurysms. *Clin Neurol Neurosurg*. 1993;95(3):205-214.

Supplemental digital content *is available for this article at neurosurgery-online.com.*

Supplemental Method: Method Pipeline and Additional Method Details.
Supplemental Table: Size stratification analysis on groups of small, medium, and large-sized aneurysms. Univariate statistical analysis for selected Mapper, established, and radiomics parameters for rupture status discrimination. The most performant features from Table 1 (AUC >0.70) were selected for this analysis. Shown are mean and standard deviation. * indicates statistical significance (assumed for $P < .05$). AUC area under the receiver operating characteristics curve.

COMMENTS

The authors present an interesting paper using "Mapper," to identify topological signatures that may predispose to aneurysm rupture.

This proof-of-concept study can be appreciated as part of a larger, growing trend of using advanced image-based analytical methods to quantify the geometrics of aneurysms, which for decades remained almost exclusively descriptive.[1a] The recent introduction of AI-based metrics, making their way into the frontline of many fields of medicine, represents the next stage in the evolution of accurate and personalized care for patients with cerebral aneurysms.[2a]

A joint multidisciplinary effort driven by computational fluid dynamics, image-processing, and pattern recognition could provide insight into aneurysm hemodynamics. Importantly, force vectors which cannot be measured directly could be inferred based on aneurysm morphology, which can be captured at a high-resolution easily and quickly.[3a]

Two major challenges that can impede the progress of future such AI-based modalities are as follows: First, the accuracy of these models is heavily reliant on and sensitive to the training data sets.[4a] As such, it is important to create multicenter and, ideally, international data-based pools, which could both increase the variability of the data feeding the model as well as create a level playing field.

Second, as analytic tools become more complex, the ability of clinicians to comprehend the output of the supporting tools, both in everyday practice as well as in an academic setting, and to decide which tools are most suitable, may be limited. Thus, in order to prevent a divide, where such papers might appear preferentially in nonclinical journals, some introductory training for academic neurosurgeons can be beneficial, much like was done for medical professionals regarding "evidence-based medicine" in previous decades.

Exemplified by this paper, in which larger dissimilarity scores were higher in ruptured vs unruptured aneurysms, the actual importance of the finding is difficult to apply directly to a specific clinical setting. The importance of this study, however, may lie in the prospect of what it offers: a look into the future of aneurysm rupture risk prediction, which undoubtedly will be formed by a set of algorithms that can trace back "disturbed" hemodynamics to specific geometric patterns.

Omer Doron,
Christopher J. Stapleton
Boston, Massachusetts, USA

1a. Juchler N, Schilling S, Glüge S, et al. Radiomics approach to quantify shape irregularity from crowd-based qualitative assessment of intracranial aneurysms. *Comput Methods Biomech Biomed Eng Imaging Vis*. 2020;8(5):538-546.
2a. Juchler N, Schilling S, Bijlenga P, Kurtcuoglu V, Hirsch S. Shape trumps size: image-based morphological analysis reveals that the 3D shape discriminates intracranial aneurysm disease status better than aneurysm size. *Front Neurol*. 2022;778.
3a. Nogata F, Yokota Y, Kawamura Y. Towards the application of AI technology to assess risk of aneurysm rupture based on medical imaging. *Int J Comput Inf Technol*. 2019;8:121-130.
4a. Alwalid O, Long X, Xie M, Han P. Artificial intelligence applications in intracranial aneurysm: achievements, challenges and opportunities. *Acad Radiol*. 2022;29:s201-s214.

© Congress of Neurological Surgeons 2023. Unauthorized reproduction of this article is prohibited.